Multiple unidirectional forward scattering of hybrid metal-dielectric nanoantenna in the near-infrared region

MU, Haiwei; LV, Jingwei; ZHANG, Xiaoming; LU, Xili; LIU, Wei; LIU, Qiang; WANG, Famei; YANG, Lin; LIU, Chao; SUN, Tao; CHU, Paul K.

Published in:
Optical Materials Express

Published: 01/11/2018

Document Version:
Final Published version, also known as Publisher's PDF, Publisher's Final version or Version of Record

Published version (DOI):
10.1364/OME.8.003410

Publication details:
MU, H., LV, J., ZHANG, X., LU, X., LIU, W., LIU, Q., WANG, F., YANG, L., LIU, C., SUN, T., & CHU, P. K. (2018). Multiple unidirectional forward scattering of hybrid metal-dielectric nanoantenna in the near-infrared region. *Optical Materials Express*, *8*(11), 3410-3423. https://doi.org/10.1364/OME.8.003410

Research Article | Vol. 8, No. 11 | 1 Nov 2018 | OPTICAL MATERIALS EXPRESS 3410
Optical Materials EXPRESS

Multiple unidirectional forward scattering of hybrid metal-dielectric nanoantenna in the near-infrared region

HAIWEI MU,[1] JINGWEI LV,[1] XIAOMING ZHANG,[2] XILI LU,[3] WEI LIU,[1] QIANG LIU,[1] FAMEI WANG,[3] LIN YANG,[1] CHAO LIU,[1,*] TAO SUN,[4] AND PAUL K. CHU[5]

[1]*School of Electronics Science, Northeast Petroleum University, Daqing 163318, China*
[2]*Institute of Dongguan-Tongji University, Dongguan, 523808, China*
[3]*School of Materials Science and Chemical Engineering, Harbin Engineering, Harbin 150001, China*
[4]*Media Lab, Massachusetts Institute of Technology, Cambridge, MA 02139, USA*
[5]*Department of Physics and Department of Materials Science and Engineering, City University of Hong Kong, Tat Chee Avenue, Kowloon, Hong Kong, China*
[*]*msm-liu@126.com*

Abstract: Direct interference between the induced magnetic and electric moments in a hybrid metal-dielectric nanodisk is demonstrated for the realization of unidirectional forward scattering in the near-infrared region. Specifically, the unidirectional forward scattering with high efficiency of the designed nanoantennas is not limited to one specific wavelength but can fit multiwavelengths. The scattering properties of the metal-dielectric hybrid nanodisk at a specific wavelength can be adjusted to meet the Kerker's type condition. In addition, the simulated optical properties of the nanoantennas reveal that the nanodisk arranged in an array exhibits efficient absorption leading to enhanced directionality. Our results provide insights into the design and engineering of highly directive nanoantennas.

1. Introduction

Scattering of electromagnetic waves at the subwavelength scale is of paramount significance in multiple areas such as nanoantennas, nanophotonics, and nanoplasmonics sensing [1–4]. Especially in scattering applications, it has been demonstrated that the scattering response of nanoantennas can be promoted by exciting magnetic dipole (MD) and electric dipole (ED) resonances [5,6]. Spectral positions of the electric and magnetic resonant responses of nanoantennas can be tailored by varying the size, shape and materials to investigate intriguing scattering phenomena such as superscattering [7], cloaking [8], and enhanced directionality [9,10].

In recently years, much research has focused on unidirectional scattering that originates from coupling between different multi-mode resonances. It is generally accepted that unidirectional scattering can be positioned on the constructive or destructive interference in the forward or backward direction [11,12]. To achieve ultra-directional enhanced forward scattering, unusual radiation patterns of scattering were theoretically proposed by Kerker through spectral overlaps of the ED and MD modes [13,14]. Owing to the superior directional scattering capability, ultra-directional Kerker's-type scattering of dielectric and metallic nanoantennas has been explored widely [15,16].

Recently, inspired by the emerging field of nanoantennas, there is growing interest in exploring artificial magnetic resonances of metallic nanostructures that can concentrate and manipulate light into nanometric volumes [17]. By virtue of the electromagnetic reciprocity, metallic nanoantennas mediate the interaction between nearby emitters and far-field radiation together with intrinsic electrical resonance in order to accomplish unidirectional forward scattering [18]. However, the high intrinsic ohmic loss is a parasitic disadvantage

#342542 https://doi.org/10.1364/OME.8.003410
Journal © 2018 Received 20 Aug 2018; revised 1 Oct 2018; accepted 5 Oct 2018; published 17 Oct 2018

Optical Materials EXPRESS

compromising the performance in the visible and near-infrared regimes [19]. To overcome this hurdle, high-index dielectric nanoantennas with low dissipative losses are attractive alternative implementation in subwavelength optics [20]. In particular, metal-dielectric core-shell nanoantennas support ED and MD resonances simultaneously inside the nanoparticles. The engineered far-field optically interference create highly directive radiation patterns with low loss and augment the degree of freedom [21]. Ge et al. and Alaee et al. investigated the unidirectional scattering of different nanostructures and found that the enhanced forward scattering of these nanoantennas can be achieved to one specific wavelength [5,11]. Moreover, it is of particular interest to achieve multiwavelength unidirectional responses.

Herein, we describe a novel hybrid metal-dielectric nanoantenna which can support both the ED and MD modes. The ED and MD modes excited in the antenna can satisfy the Kerker's type condition. More specifically, our results show that the unidirectional forward scattering can be achieved by adjusting the geometric parameters of the nanoantenna, which is not limited to one specific wavelength but can fit in the multiple wavelength band. Furthermore, directionality can be improved by a 1D chain and multiple unidirectional scattering can also be achieved when the core-shell nanodisk is excited by a near-field dipole source.

2. Multipole composition method

We consider the scattering properties of the hybrid core-shell nanodisk using the multipole decomposition method when the resonant contributions from different multipoles are tuned to overlap spectrally [22]. To clarify the contributions of different modes, multipole decomposition including the electric dipole moment **P** (ED), magnetic dipole moment **M** (MD), toroidal dipole moment **T** (TD), electric quadrupole moment $\hat{Q}'$ (EQ), and magnetic quadrupole moment $\hat{M}'$ (MQ) is considered as follows [23].

$$\mathbf{p} = \int \mathbf{P}(\mathbf{r}')\mathrm{d}\mathbf{r}' \tag{1}$$

$$\mathbf{m} = -\frac{i\omega}{2}\int [\mathbf{r}'\times\mathbf{P}(\mathbf{r}')]d\mathbf{r}' \tag{2}$$

$$\mathbf{T} = \frac{i\omega}{10}\int [(2\mathbf{r}'^2\mathbf{P}(\mathbf{r}') - (\mathbf{r}'\cdot\mathbf{P}(\mathbf{r}'))\mathbf{r}']d\mathbf{r}' \tag{3}$$

$$\hat{Q}' = \hat{Q} + \hat{Q}'' \tag{4}$$

$$\hat{Q} = 3\int [\mathbf{r}'\mathbf{P}(\mathbf{r}') + \mathbf{P}(\mathbf{r}')\mathbf{r}' - \frac{2}{3}[\mathbf{r}'\cdot\mathbf{P}(\mathbf{r}')]\hat{U}]d\mathbf{r}' \tag{5}$$

$\hat{Q}$ is the irreducible tensor of the electric quadrupole moment ($\hat{U}$ is the 3×3 unit tensor), and

$$\hat{Q}'' = 2\int [\mathbf{r}'\cdot\mathbf{P}(\mathbf{r}')]\hat{U}d\mathbf{r}' \tag{6}$$

$$\hat{M}' = \hat{M} + \hat{M}'' \tag{7}$$

$\hat{M}$ is the irreducible tensor of the magnetic quadrupole moment

$$\hat{M} = \frac{\omega}{3i}\int \{\mathbf{r}'\times\mathbf{P}(\mathbf{r}')]\mathbf{r}' + \mathbf{r}'[\mathbf{r}'\times\mathbf{P}(\mathbf{r}')]\}d\mathbf{r}' \tag{8}$$

and the components of the asymmetric tensor

$$\hat{M}'' = \frac{\omega}{3i}\int \{\mathbf{r}'\times\mathbf{P}(\mathbf{r}')]\mathbf{r}' - \mathbf{r}'[\mathbf{r}'\times\mathbf{P}(\mathbf{r}')]\}d\mathbf{r}' \tag{9}$$

Optical Materials EXPRESS

where $\mathbf{P}(\mathbf{r}')$ is the polarization induced in the scatter by an incident light wave and $\mathbf{r}'$ is the radius-vector of a volume element inside the scattering medium. Multipole contributions show that the resonance peaks correspond to the overlap of several different multipole decomposition of the scattered field. The radiation power I from these different multipole moments can be achieved as follows [24]:

$$I = \frac{1}{4\pi\varepsilon_0}[\frac{2\omega^4}{3c^3}|\mathbf{P}|^2 + \frac{2\omega^4}{3c^3}|\mathbf{M}|^2 + \frac{4\omega^5}{3c^4}\mathrm{Im}(\mathbf{P}\cdot\mathbf{T}^*) + \frac{2\omega^6}{3C^5}|\mathbf{T}|^2 + \frac{\omega^6}{20c^5}|\mathbf{Q}^e|^2 + \frac{\omega^6}{20c^5}|\mathbf{Q}^m|^2] \tag{10}$$

$$C_{sca} = \frac{I}{I_{inc}} \tag{11}$$

where I_{inc} is the radiation power of the incident light wave.

3. Results and discussions

The hybrid metal-dielectric nanodisk is schematically shown in Fig. 1. The radii of the silicon outer hollow nanodisk and gold inner nanodisk are R = 120 nm and r_1 = 48 nm with a height of H = 220 nm. In the hybrid nanoantennas, the Si and Au nanodisk are placed closely together to form the hybrid nanodisk with a gap distance of r- r_1 = 2 nm. In the simulation, a plane wave impinges onto the hybrid nanodisk along the x direction with E_y polarization. The hybrid nanodisk is embedded in a homogenous host medium with a gold core (dielectric functions extracted from Palik's handbook [25]) and dielectric shell (the refractive index of n = 3.5). The scattering properties are investigated by the finite element method by COMSOL Multiphysics [26].

We first investigate the scattering properties of an individual silicon hollow nanodisk. Figure 2(a) shows the multipole contributions to the scattering cross-section of the hollow nanodisk with H = 220 nm, R = 120 nm, r = 50 nm. These resonances correspond to wavelengths of 698 nm and 937 nm, which can be considered as the overlap of the resonant contributions of several different multipoles. The method of scattering cross-section multipole decomposition is implemented to interpret the peaks of the hollow nanodisk [27]. It is clear that a sharp peak at 937 nm originates from the magnetic dipole (MD) whereas the broad one at 698 nm is ascribed to the electric dipole (ED) resonance. Moreover, the MD and ED are dominant over the whole spectrum and the contributions of toroidal dipole moment (TD), electric quadrupole moment (EQ), and magnetic quadrupole moment (MQ) are negligible in the system. Hence, we will only consider the individual silicon hollow nanodisk with the contributions of the MD and ED because of the scattering features. To elucidate the underlying scattering mechanism, the real and imaginary components of the electric and magnetic moments are depicted in Fig. 2(b). To unambiguously clarify the contributions from different modes, the radiated far-field of the nanoantennas with an induced electric dipole moment p_y (ED), magnetic dipole moment m_z (MD) are considered as follows [23]:

Optical Materials EXPRESS

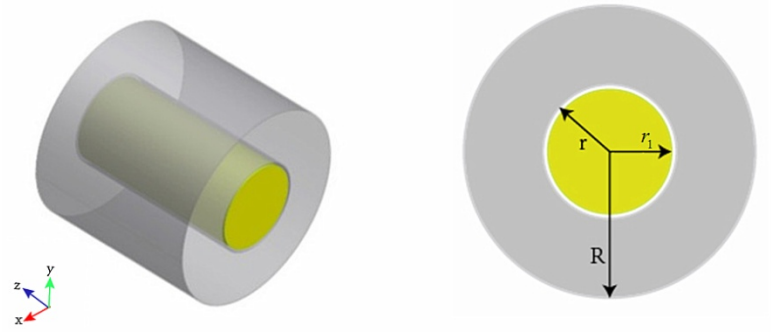

Fig. 1. Schematic illustration of the metal-dielectric hybrid nanodisk.

$$\mathbf{E}_{\text{far}}(\mathbf{r}) = \frac{k^2}{4\pi\varepsilon} p_y \frac{e^{ikr}}{r}(-\sin\varphi\hat{\varphi} + \cos\theta\cos\varphi\hat{\theta}) \\ -\frac{Zk^2}{4\pi} m_z \frac{e^{ikr}}{r}(\cos\theta\sin\varphi\hat{\varphi} - \cos\varphi\hat{\theta}) + \ldots \tag{12}$$

where r, θ, and ϕ are the spherical coordinates. The backward scattering cross-section of the nanoantennas can be defined as [5]

$$\sigma_{\text{BW}} = \lim_{r\to\infty} 4\pi r^2 \frac{\left|\mathbf{E}_{\text{far}}(\varphi = 0, \theta = \pi)\right|^2}{\left|\mathbf{E}_{\text{inc}}\right|^2} \\ = \frac{k^4}{4\pi\varepsilon^2 \left|\mathbf{E}_{\text{inc}}\right|^2}\left|p_y - \frac{\sqrt{\varepsilon_r} m_z}{c}\right| \tag{13}$$

Backward scattering can be exterminated if the Kerker condition is satisfied:

$$p_y - \frac{\sqrt{\varepsilon_r} m_z}{c} = 0 \tag{14}$$

$$p_y = \frac{m_z}{c} \tag{15}$$

At the wavelength of 1034 nm, the real and imaginary components of the MD and ED are almost the same thus satisfying the Kerker's-type condition. Thus, they constructively interfere in the far field, leading to the dramatic enhancement in unidirectional forward scattering and suppression of backward scattering.

Optical Materials EXPRESS

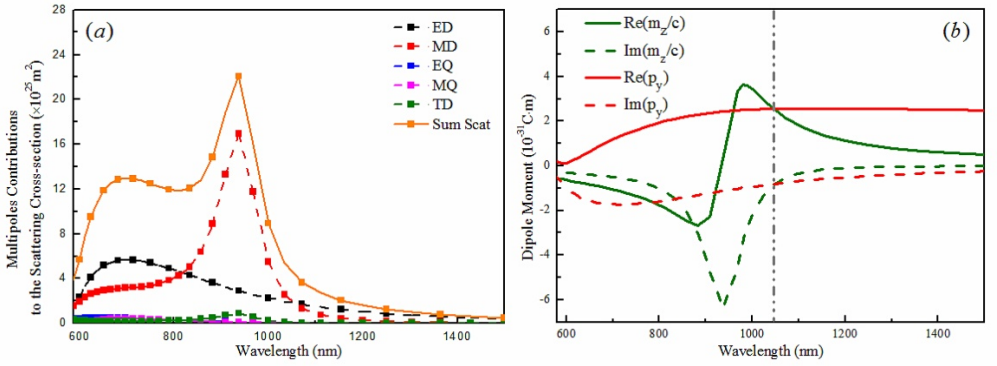

Fig. 2. (a) Multipole contributions to the scattering cross-section and (b) Real and imaginary components of the electric and magnetic moments of individual silicon hollow nanodisk with H = 220 nm, R = 120 nm, r = 50 nm.

Figure 3 shows the forward, backward scattering, and ratio between forward and backward scattering (FS/BS ratio) for the investigated nanoantennas. Forward scattering and backward scattering are determined as an integral of Poynting's vector in the semi-space with $x > 0$ and $x < 0$. It is obvious that the scattering intensity for the FS and BS are quite different and the maximum ratio of the FS to BS intensity appears at 1034 nm, at which the scattering intensity of BS is the minimum. The peak ratio of the FS to BS intensity is approximately 7.5, indicating that forward scattering is substantially enhanced due to interference of the MD and ED. The inset in the 3D far-field scattering pattern at the wavelength of 1034 nm shows more significant attenuation of the BS corresponding to the Kerker's-type scattering (see Fig. 2(b)). It is clear that the unidirectional FS can be realized in the individual hollow silicon nanodisk.

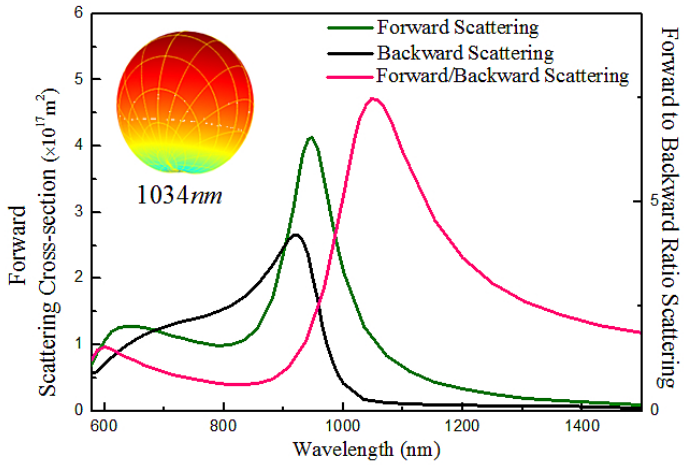

Fig. 3. Forward and backward scattering and forward/backward ratio scattering spectra for the individual hollow silicon nanodisk with H = 220 nm, R = 120 nm, r = 50 nm.

An accurate analysis of the multipole contributions to the scattering cross-section of the isolated Au nanodisk with r = 48 nm and H = 220 nm is performed as shown in Fig. 4(a). There is a relatively sharp resonance band at about 545 nm, correlating with different multipole resonances such as the electric dipole, magnetic dipole and toroidal dipole. Figure 4(b) shows the forward and backward radar scattering cross-sections for the individual Au nanodisk. The cross-sections of the FS and BS are similar over the whole spectrum because of

Optical Materials EXPRESS

the dominating dipolar response. Moreover, the FS and BS provide pronounced peak at the wavelength of 545 nm, which corresponds to the maximum total scattering cross section.

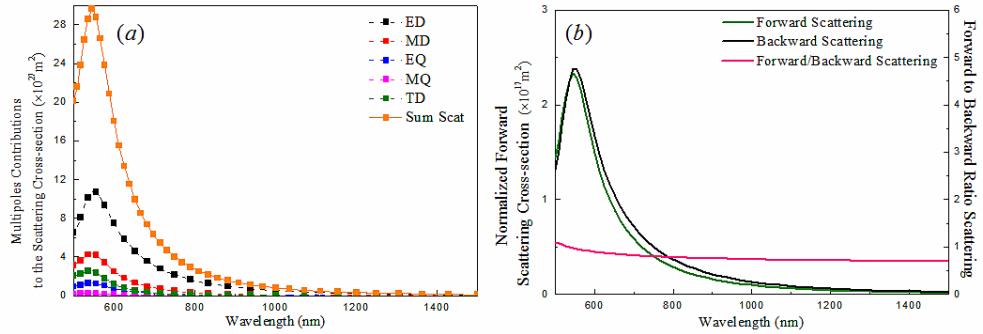

Fig. 4. (a) Multipole contributions to the scattering cross-section and (b) Forward and backward scattering and forward/backward ratio scattering spectra of the individual Au nanodisk with H = 220 nm, r = 48 nm.

When the Au nanodisk with the radius of r_1 = 50 nm and H = 220 nm is introduced into the center of the aforementioned Si hollow nanodisk, the multipole contributions to the scattering cross-section of core-shell nanodisk are depicted in Fig. 5(a). Three resonances are visible at $\lambda = 750nm$, $\lambda = 909nm$ and $\lambda = 1071nm$, which correspond to the overlap of the resonant contributions from the ED and MD. Negligible contributions from the higher order multipolar moments are also presented in the total scattering efficiency spectrum. Moreover, the magnetic dipole resonance and electric dipole resonance from the core-shell nanodisk coincide spectrally, resulting in a distinct asymmetric dip at 970 nm on the base of coherent interference [28]. The ratio between the FS and BS for the core-shell nandisk is shown in Fig. 5(b). The resonant peaks of the forward scattering correspond to the maximum scattering cross section and it is caused by the interference of the electric and magnetic dipolar modes in this system. Strong suppression of backward scattering is realized in the resonant region for wavelengths between 770 nm and 960 nm due to destructive far-field interference. Figure 5(c) depicts the scattered field patterns in the *xoy* plane at the wavelengths corresponding to the maximum of the FS/BS. It is observed that backward scattering is stronger than forward scattering at $\lambda = 750nm$, and backward scattering is not completely suppressed at $\lambda = 909nm$ and $\lambda = 1071nm$. Therefore, scattering at the vanishing backward direction cannot be neglected and it does not meet the Kerker's-type condition.

Optical Materials EXPRESS

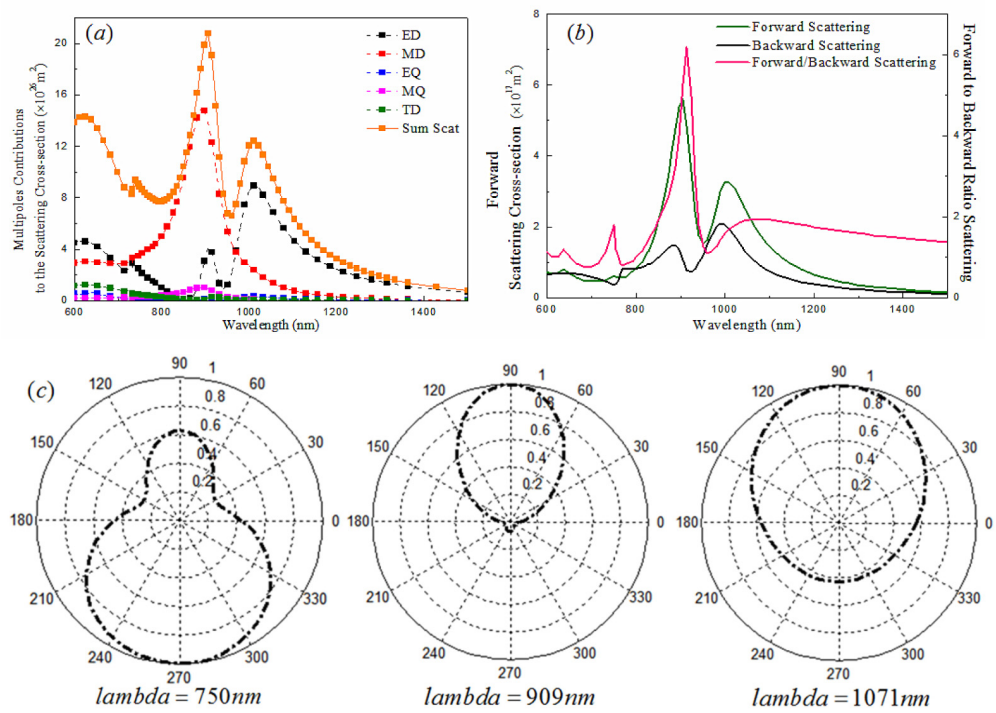

Fig. 5. (a) Multipole contributions to the scattering cross-section, (b) Forward and backward scattering and forward/backward ratio scattering spectra, and (c) Scattered field pattern of core-shell nanodisk. The core nanodisk is made of gold of H = 220 nm, r_1 = 50 nm, r = 50 nm and the shell is the n = 3.5 dielectric with radius R = 120 nm.

In order to meet the Kerker's type condition, the directive hybrid core-shell nanoantennas with zero backscattering is designed. In this configuration, the Si and Au nanodisks are placed close to each other at a gap of r-r_1 = 2 nm. To analyze the physical mechanism of unidirectional scattering, the scattering cross-section of multipole modes is given in Fig. 6(a). Two types of multipole moments in this system are efficiently excited. One mode with a resonance wavelength $\lambda = 891nm$ shows a resonant peak of the ED and MD moment. The ED moment is identical to the magnetic dipole moment at the overlapping resonant point $\lambda = 952nm$. It is clear that the Kerker's type condition is met at the wavelength of $\lambda = 952nm$, where the electric and magnetic dipole moments are identical in phase and amplitude. To verify the accuracy of the total scattering cross-section of the hollow nanodisk, we compare the simulation results of spectra of the scattering cross-section and the results calculated by multipole decomposition are plotted in Fig. 6(b). The calculated spectrum of the scattering cross-section (SCS, see the red solid line) is simulated with the finite element method by COMSOL Multiphysics. The total scattering cross-section (Total, see the black solid line) can be regard as the sum scattering of the ED, MD, MQ, EQ and TD. There is excellent agreement with the total SCSs of the ED, MD, MQ, EQ and TD, which is obtained by the FEM method. However, it is noted that there is discrepancy at the resonance wavelength of 891 nm due to the interference term between electric dipole and toroidal dipole in Eq. (10). The role of the interference term may contribute significantly to the scattering. This is an important feature which can help us understand the mode couplings in our metal-dielectric system. The forward/backward ratio scattering spectrum is described in Fig. 6(c). There are two spectral peaks at $\lambda = 804nm$ and $\lambda = 924nm$, indicating more substantial suppression of backward scattering at the spectral wavelength. Therefore, the destructive and constructive inferences of the radiated fields are because the ED and MD moments of

Optical Materials EXPRESS

scattering dramatically suppress and enhance the BS and FS. Coupling between the ED and MD for the enhanced scattering response on the core-shell nanodisk can be interpreted by analyzing the underlying mechanism of multipolar modes. According to Eq. (9), BS can be fully eliminated when the Kerker condition is fulfilled: $p_y = \frac{m_z}{c}$. The wavelength dependence of the real and the imaginary components is depicted in Fig. 6(d). It can be seen that the real and imaginary components of the MD and ED are identical at the wavelength of 952 nm, meaning that the Kerker's type conditions can be fulfilled and unidirectional FS can be achieved. Besides, there is an approximate equivalent real and imaginary components of the MD and ED at the wavelength of 804 nm, which creates a point to approximately realize the Kerker's type condition. Thus, unidirectional forward scattering is obtained for the multipolar modes corresponding to realization of the Kerker's type conditions in the near-infrared region.

In addition, the optical properties of hybrid nanodisks placed close to each other at a gap of 2 nm can lead to enhanced scattering directivity in Fig. 6, compared with hybrid core-shell nanodisk without a gap in Fig. 5. This can be explained that the scattering in Fig. 5 at the vanishing backward direction cannot be neglected and the forward scattering is not dramatically enhanced at the wavelengths of the FS/BS to achieve the unidirectional forward scattering. From another point of view, the unidirectional forward scattering is realized when the gap size increases from 0 nm to 2 nm and the Au nanodisk is introduced into the center of the aforementioned Si hollow nanodisk, which attributes to the interaction between the Si hollow nanodisk and the isolated Au nanodisk. Therefore, it can be concluded that the gap between the Au core and the Si shell is crucial to the unidirectional scattering, and the gap size and material have remarkable impacts the scattering features of the designed nanoantenna.

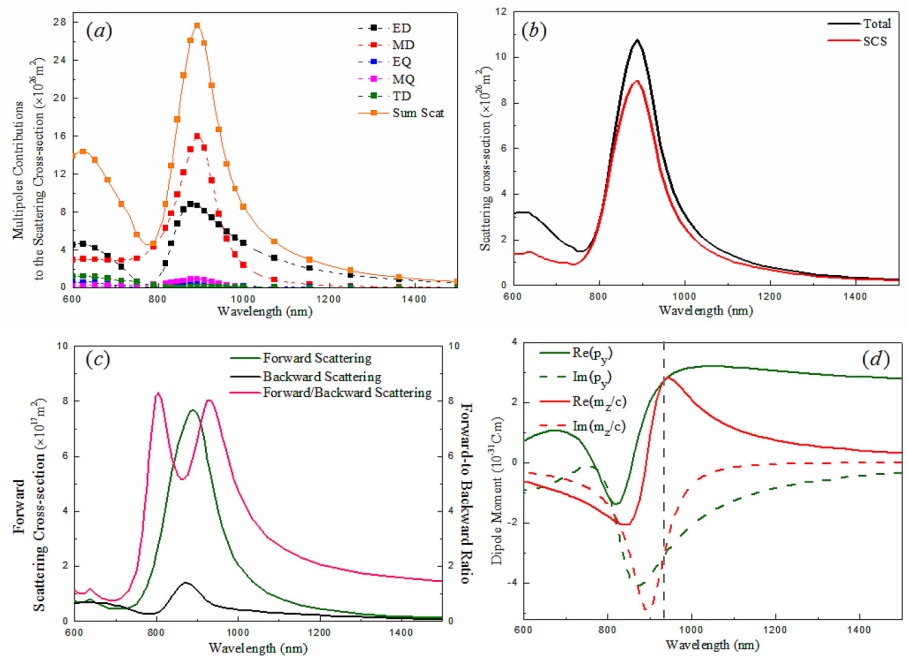

Fig. 6. (a) Multipole contributions to the scattering cross-section, (b) Comparison of the total total scattering cross-section with SCS, (c) Forward and backward scattering and forward/backward ratio scattering spectra, and (d) Real and imaginary components of the electric and magnetic moments of the core-shell nanodisk. The core nanodisk is made of gold of r_1 = 48 nm and the shell is the n = 3.5 dielectric with H = 220 nm, R = 120 nm, r = 50 nm.

Optical Materials EXPRESS

To obtain more information about the scattering properties of the core-shell nanodisk, the electric and magnetic field distribution profiles corresponding to multipole wavelengths of 804 nm, 924 nm and 952 nm are calculated and shown in Fig. 7. The blue arrows show the circulating polarization density distributions. With regard to the electric field distributions in Fig. 7(a), the electric "hottest spots" with highly enhanced near-field in the gap are obtained at multipole wavelength, which reveal the nature of electric field interactions between the ED and MD modes of the core-shell nanodisk. The magnetic hot-spots with highly enhanced localized fields are shown in Fig. 7(b). A high magnetic field intensity can be observed inside the Si hollow nanodisk as a result of the strong electromagnetic coupling between Si hollow nanodisk and Au nanodisk. The FS/BS_{max} near-field scattering patterns are associated with the magnetic resonant suppression and the interference of the ED and MD moments.

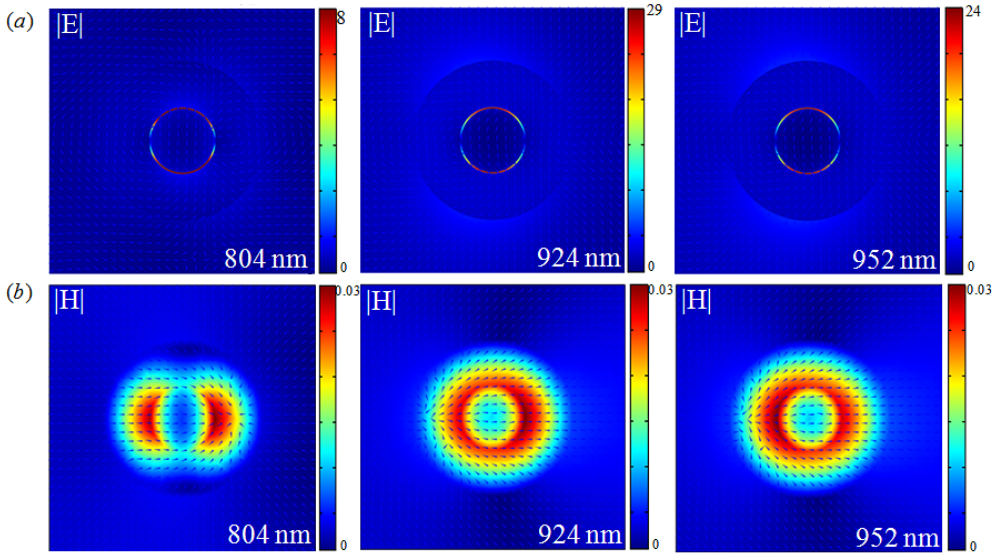

Fig. 7. Spatial profiles: (a) Elecctric field and (b) Magnetic field at the wavelengths of FS/BS_{max}

To specifically analyze backscattering suppression, the scattered field patterns of the core-shell nanodisk at multipole wavelengths are shown in Fig. 8. Scattering is substantially suppressed in the backward direction and dramatically enhanced in the forward direction. In addition, vanishing backscattering in this spectral region is achieved by overlapping of the MD and ED to satisfy the Kerker's type condition at the wavelength of $\lambda = 952nm$. On the other hand, the radiated far fields are in phase with forward scattering and no backscattering is obtained due to the destructive interference between these multipolar resonant moments [29]. Hence, we note that multiple unidirectional forward scattering in the near-infrared region can be modulated by overlapping the resonant contributions of several different multipolar moments, when the Si and Au nanodisks are placed close to each other at a gap of $r\text{-}r_1 = 2$ nm.

Optical Materials EXPRESS

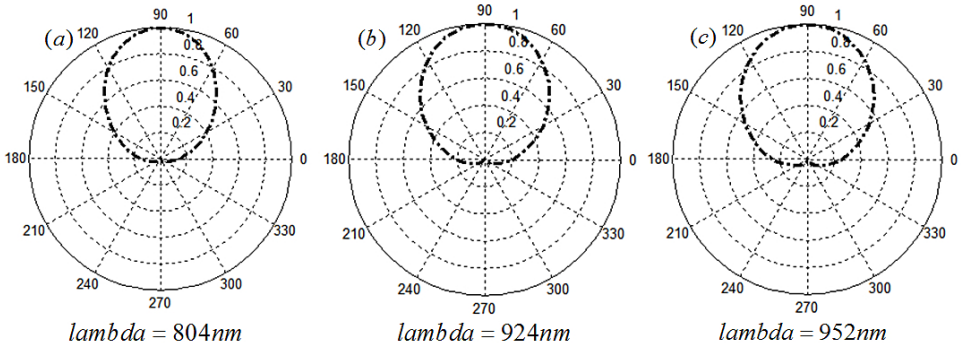

Fig. 8. Scattered field pattern of the core-shell nanodisk with H = 220 nm, R = 120 nm, r = 50 nm, rr = 48 nm calculated at the wavelength 804 nm and 924 nm. The angle of 90° (270°) corresponds to the forward (backward) direction.

To compare the enhanced directionality in the scattering response of various nanoantennas, the forward/backward ratio scattering spectra for the Si hollow nanodisk, Au nanodisk, and core-shell nanodisk are investigated and the results are shown in Fig. 9. The spectra of the scattering intensity for the FS/BS are quite different. The maximum ratio of the FS to BS intensity appears at wavelengths of 804 nm and 924 nm for the core-shell nanodisk, while the scattering intensities of the Si hollow nanodisk and the Au nanodisk maintain a minimum value. Furthermore, the ratio of the FS to BS intensity is approximately 8.3 for the core-shell nanodisk and it is larger than the ratio of the Si hollow nanodisk and Au nanodisk. In this case, the core-shell nanodisk can provide favorable directionality to realize the controllability of the scattering characteristics.

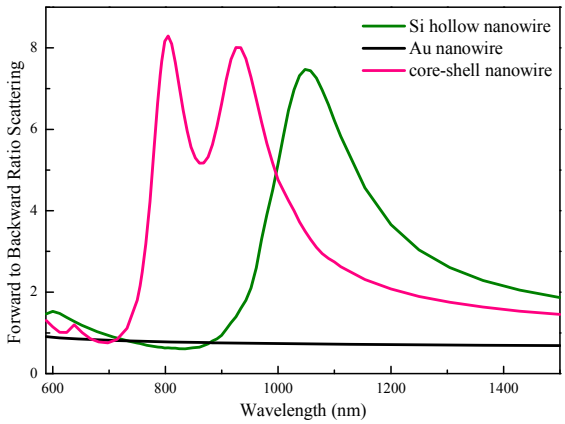

Fig. 9. Forward/backward ratio scattering spectra of the Si hollow nanodisk, Au nanodisk, and core-shell nanodisk with H = 220 nm, R = 120 nm, r = 50 nm, r_1 = 48 nm.

Apart from the excitation of plane wave, it is desirable to investigate the unidirectional scattering in the core-shell nanodisk for a nearby electric dipole emitter. The far-field forward-to-backward directionality can be defined as $G_{FB} = 10\log_{10}(S_F / S_B)$, where S_F is the amplitude of the power radiated in forward scattering (90°) and backscattering (270°) [30,31]. Figure 10 presents the G_{FB} spectrum as a function of the electric dipole placed at the center to the bottom of nanoantennas along the y axis with a distance d and wavelength λ. As shown in Fig. 10, G_{FB} for the core-shell nanodisk can reach about 7.8 dB and remain the same as d changes from 0 nm to 40 nm. The emission pattern of the hybrid nanoantennas

Optical Materials EXPRESS

changes slightly when the displacement of the electric dipole is in the range of several ten nanometers. The peak positions of G_{FB} slightly blue-shifts due to the difference between near and far-field illumination [32]. Moreover, the G_{FB} spectra in Fig. 10 show that it is nearly zero at the wavelength of 795 nm due to sole ED excitation when the electric dipole emitter is located at the center of the hybrid core-shell nanodisk [33].

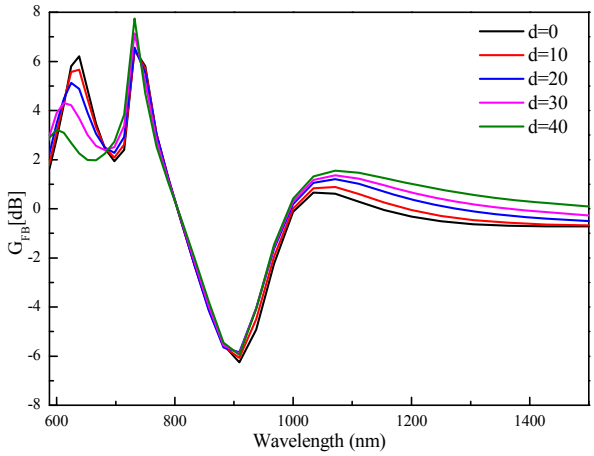

Fig. 10. Far-field forward-to-backward directionality $G_{FS/BS_{max}}$ for electric dipole excitation.

Figure 11 illustrates the unidirectionality of the core-shell nanodisk with a linear chain along the x axis. There are three wavelengths corresponding to the resonant wavelengths of a single hybrid core-shell nanodisk at $\lambda = 804nm$, $\lambda = 924nm$ and $\lambda = 952nm$. A drastic change in the emission pattern is observed due to the ED and MD with scattering cross-sections interference and hence, almost complete cancellation of backscattering is obtained. The increase in directionality for an increasing number of nanoantennas N is clearly visible due to constructive far-field interference [34]. As a result, the unidirectional scattering properties can be observed from the hybrid metal-dielectric nanodisk with a linear chain.

Optical Materials EXPRESS

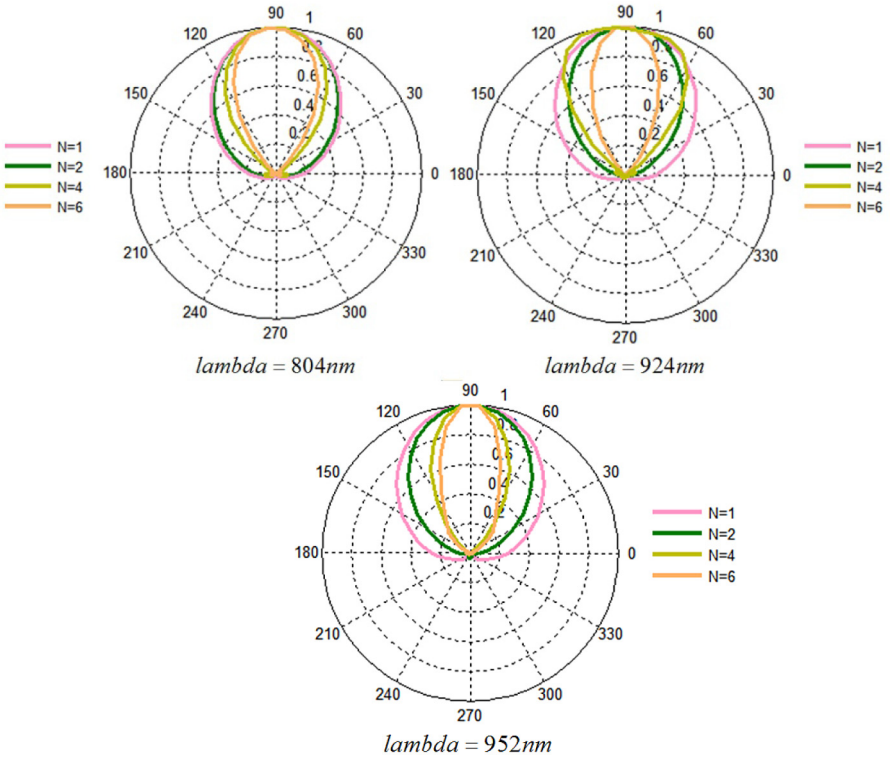

Fig. 11. Scattering pattern by an array of nanoantennas with N = 1, 2, 4, 6.

4. Conclusion

A highly unidirectional hybrid core-shell nanodisk is designed and investigated by the multipole composition method. The simulated scattering line shape is obtained by calculating the probability to simultaneously excite the electromagnetic ED and MD moments in the forward and backward directions and the multiple unidirectional forward scattering can be realized. Our study summarizes the Kerker's type condition for vanishing backward scattering, which arises from constructive and destructive interference of different multipolar moments. An array of nanodisks with enhanced directionality exhibits a predictive feature for close-by magnetic dipoles. The electromagnetic resonance with highly unidirectionality and controllability spurs applications in sensing, nanoantennas and nanophotonics.

Funding

National Natural Science Foundation of China (Grant No. 51474069, 41472126); China Postdoctoral Science Foundation funded project (Grant No. 2016M591510); Natural Science Foundation of Heilongjiang Province (Grant No. E2016007, E2017010); Northeast Petroleum University Innovation Foundation For Postgraduate (Grant No. YJSCX2017-034NEPU); Hong Kong Research Grants Council (RGC) General Research Funds (GRF) (No. CityU 11205617); City University of Hong Kong Applied Research Grant (ARG) No. 9667122.

References

1. D. Sikdar, W. Cheng, and M. Premaratne, "Optically resonant magneto-electric cubic nanoantennas for ultra-directional light scattering," J. Appl. Phys. **117**(8), 083101 (2015).
2. H. Alisafaee and M. A. Fiddy, "Nanoantennas for nanodisk photovoltaics," Appl. Phys. Lett. **105**(11), 113107 (2014).

Optical Materials EXPRESS

3. W. Wan, W. Zheng, Y. Chen, and Z. Liu, "From Fano-like interference to superscattering with a single metallic nanodisk," Nanoscale **6**(15), 9093–9102 (2014).
4. M. E. Stewart, C. R. Anderton, L. B. Thompson, J. Maria, S. K. Gray, J. A. Rogers, and R. G. Nuzzo, "Nanostructured Plasmonic Sensors," Chem. Rev. **108**(2), 494–521 (2008).
5. R. Alaee, R. Filter, D. Lehr, F. Lederer, and C. Rockstuhl, "A generalized Kerker condition for highly directive nanoantennas," Opt. Lett. **40**(11), 2645–2648 (2015).
6. R. Alaee, C. Menzel, U. Huebner, E. Pshenay-Severin, S. Bin Hasan, T. Pertsch, C. Rockstuhl, and F. Lederer, "Deep-subwavelength plasmonic nanoresonators exploiting extreme coupling," Nano Lett. **13**(8), 3482–3486 (2013).
7. L. Verslegers, Z. Yu, Z. Ruan, P. B. Catrysse, and S. Fan, "From electromagnetically induced transparency to superscattering with a single structure: a coupled-mode theory for doubly resonant structures," Phys. Rev. Lett. **108**(8), 083902 (2012).
8. Y. J. Feng, S. Xiong, X. F. Xu, B. Zhu, J. M. Zhao, and T. Jiang, "Dielectric multilayers for antenna and cloaking devices designed from transformation electromagnetics," Ursi International Symposium on Electromagnetic Theory, 872–875, (2013).
9. A. E. Krasnok, A. E. Miroshnichenko, P. A. Belov, and Y. S. Kivshar, "All-dielectric optical nanoantennas," Opt. Express **20**(18), 20599–20604 (2012).
10. S. Person, M. Jain, Z. Lapin, J. J. Sáenz, G. Wicks, and L. Novotny, "Demonstration of zero optical backscattering from single nanoparticles," Nano Lett. **13**(4), 1806–1809 (2013).
11. L. Ge, L. Liu, S. Dai, J. Chai, Q. Song, H. Xiang, and D. Han, "Unidirectional scattering induced by the toroidal dipolar excitation in the system of plasmonic nanoparticles," Opt. Express **25**(10), 10853–10862 (2017).
12. F. Qin, Q. Zhang, and J. J. Xiao, "Sub-wavelength unidirectional antenna realized by stacked spoof localized surface plasmon resonators," Sci. Rep. **6**(1), 29773 (2016).
13. M. Kerker, D. S. Wang, and C. L. Giles, "Electromagnetic scattering by magnetic spheres," J. Opt. Soc. Am. **73**(6), 765–767 (1983).
14. J. M. Geffrin, B. García-Cámara, R. Gómez-Medina, P. Albella, L. S. Froufe-Pérez, C. Eyraud, A. Litman, R. Vaillon, F. González, M. Nieto-Vesperinas, J. J. Sáenz and F. Moreno, "Magnetic and Electric Coherence in Forward- and Back-Scattered Electromagnetic Waves by a Single Dielectric Subwavelength Sphere," Nat. Commun. **3**, 1171 (2012).
15. W. J. Luyten, "Directional emission from a single plasmonic scatterer," Nat. Commun. **5**, 3250 (2014).
16. R. Alaee, M. Albooyeh, M. Yazdi, N. Komjani, C. Simovski, F. Lederer, and C. Rockstuhl, "Magnetoelectric coupling in nonidentical plasmonic nanoparticles: Theory and applications," Phys. Rev. B Condens. Matter Mater. Phys. **91**(11), 115119 (2015).
17. D. K. Gramotnev and S. I. Bozhevolnyi, "Nanofocusing of electromagnetic radiation," Nat. Photonics **8**(1), 13–22 (2014).
18. Y. Yang, Q. Li, and M. Qiu, "Controlling the angular radiation of single emitters using dielectric patch nanoantennas," Appl. Phys. Lett. **2**(3), 031109 (2015).
19. T. Feng, Y. Xu, Z. Liang, and W. Zhang, "All-dielectric hollow nanodisk for tailoring magnetic dipole emission," Opt. Lett. **41**(21), 5011–5014 (2016).
20. I. Staude, A. E. Miroshnichenko, M. Decker, N. E. T. Fofang, S. Liu, E. Gonzales, J. Dominguez, T. S. Luk, D. N. Neshev, I. Brener, and Y. Kivshar, "Tailoring directional scattering through magnetic and electric resonances in subwavelength silicon nanodisk," ACS Nano **7**, 7824–7832 (2013).
21. W. Liu, A. E. Miroshnichenko, R. F. Oulton, D. N. Neshev, O. Hess, and Y. S. Kivshar, "Scattering of core-shell nanowires with the interference of electric and magnetic resonances," Opt. Lett. **38**(14), 2621–2624 (2013).
22. Q. Zhang, J. J. Xiao, M. L. Li, D. Z. Han, and L. Gao, "Core-shell-structured dielectric-metal circular nanodisk antenna: Gap plasmon assisted magnetic toroid-like cavity modes," ACS Photonics **2**(1), 60–65 (2015).
23. A. B. Evlyukhin, T. Fischer, C. Reinhardt, and B. N. Chichkov, "Optical theorem and multipole scattering of light by arbitrary shaped nanoparticles," Phys. Rev. B **94**(20), 205434 (2016).
24. X. L. Zhang, S. B. Wang, Z. F. Lin, H. B. Sun, and C. T. Chan, "Optical force on toroidal nanostructures: toroidal dipole versus renormalized electric dipole," Phys. Rev. B Condens. Matter Mater. Phys. **92**, 043804 (2015).
25. E. D. Palik, *Handbook of Optical constants of Solids* (Academic Press, New York 1985).
26. C. O. M. S. O. L. Multiphysics, 5.1 (http://www.comsol.com).
27. J. D. Jackson, *Classical Electrodynamics*, 3rd ed. (Wiley, 1998).
28. X. Ci, B. Wu, Y. Liu, G. Chen, E. Wu, and H. Zeng, "Magnetic-based Fano resonance of hybrid silicon-gold nanocavities in the near-infrared region," Opt. Express **22**(20), 23749–23758 (2014).
29. P. D. Terekhov, K. V. Baryshnikova, A. S. Shalin, A. Karabchevsky, and A. B. Evlyukhin, "Resonant forward scattering of light by high-refractive-index dielectric nanoparticles with toroidal dipole contribution," Opt. Lett. **42**(4), 835–838 (2017).
30. J. D. Kraus and R. J. Marhefka, *Antenna for all applications*, 3rd ed. (McGraw-Hill: N. Y. 2001).
31. T. Pakizeh and M. Käll, "Unidirectional Ultracompact Optical Nanoantennas," Nano Lett. **9**(6), 2343–2349 (2009).
32. P. D. Terekhov, K. V. Baryshnikova, Y. A. Artemyev, A. Karabchevsky, A. S. Shalin, and A. B. Evlyukhin, "Multipolar response of nonspherical silicon nanoparticles in the visible and near-infrared spectral ranges," Phys. Rev. B **96**(3), 035443 (2017).

Optical Materials EXPRESS

33. T. Feng, Y. Xu, Z. Liang, and W. Zhang, "All-dielectric hollow nanodisk for tailoring magnetic dipole emission," Opt. Lett. **41**(21), 5011–5014 (2016).
34. X. M. Zhang, Q. Zhang, S. J. Zeng, Z. Z. Liu, and J. J. Xiao, "Dual-band unidirectional forward scattering with all-dielectric hollow nanodisk in the visible," Opt. Lett. **43**(6), 1275–1278 (2018).